CGG repeat expansion in *LRP12* in amyotrophic lateral sclerosis

Graphical abstract

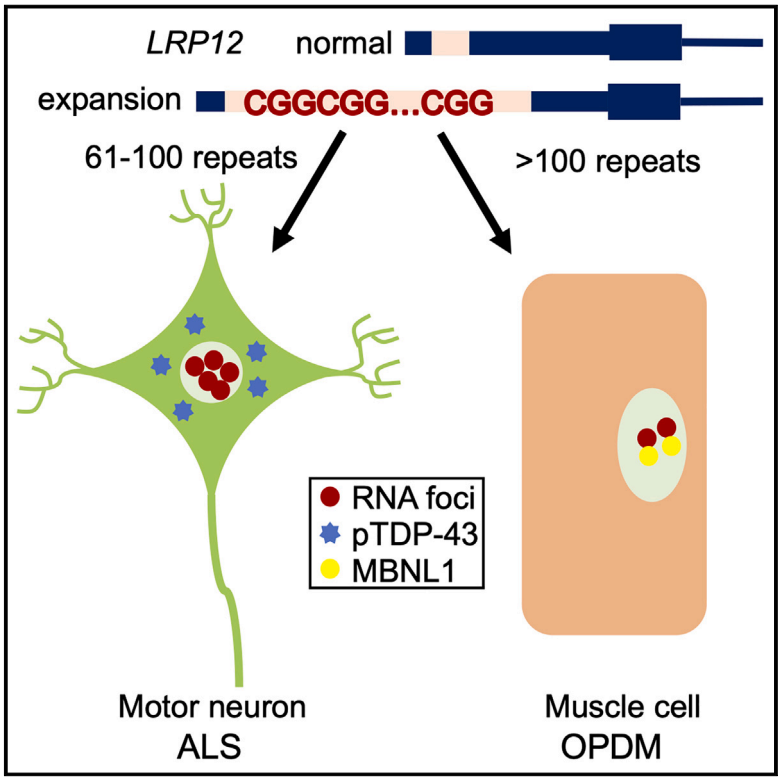

Authors

Kodai Kume, Takashi Kurashige, Keiko Muguruma, ..., Yuishin Izumi, Masashi Aoki, Hideshi Kawakami

Correspondence

hkawakam@hiroshima-u.ac.jp

We show that CGG repeat expansion in *LRP12* is a cause of amyotrophic lateral sclerosis (ALS), in addition to oculopharyngodistal myopathy (OPDM). Relatively short expansions (61–100 repeats) produce more abnormal RNA, causing an accumulation of phosphorylated TDP-43, leading to ALS. More than 100 repeats cause MBNL1 dysfunction, leading to OPDM.

Kume et al., 2023, The American Journal of Human Genetics *110*, 1086–1097
July 6, 2023
https://doi.org/10.1016/j.ajhg.2023.05.014

ARTICLE

CGG repeat expansion in *LRP12* in amyotrophic lateral sclerosis

Kodai Kume,[1,16] Takashi Kurashige,[2,16] Keiko Muguruma,[3,16] Hiroyuki Morino,[1,14] Yui Tada,[1] Mai Kikumoto,[1,4] Tatsuo Miyamoto,[5,15] Silvia Natsuko Akutsu,[5] Yukiko Matsuda,[1] Shinya Matsuura,[5] Masahiro Nakamori,[4] Ayumi Nishiyama,[6] Rumiko Izumi,[6] Tetsuya Niihori,[7] Masashi Ogasawara,[8] Nobuyuki Eura,[8] Tamaki Kato,[9] Mamoru Yokomura,[9] Yoshiaki Nakayama,[10] Hidefumi Ito,[10] Masataka Nakamura,[11] Kayoko Saito,[9] Yuichi Riku,[12] Yasushi Iwasaki,[12] Hirofumi Maruyama,[4] Yoko Aoki,[7] Ichizo Nishino,[8] Yuishin Izumi,[13] Masashi Aoki,[6] and Hideshi Kawakami[1,*]

Summary

Amyotrophic lateral sclerosis (ALS) is a neurodegenerative disorder characterized by the degeneration of motor neurons. Although repeat expansion in *C9orf72* is its most common cause, the pathogenesis of ALS isn't fully clear. In this study, we show that repeat expansion in *LRP12*, a causative variant of oculopharyngodistal myopathy type 1 (OPDM1), is a cause of ALS. We identify CGG repeat expansion in *LRP12* in five families and two simplex individuals. These ALS individuals (*LRP12*-ALS) have 61–100 repeats, which contrasts with most OPDM individuals with repeat expansion in *LRP12* (*LRP12*-OPDM), who have 100–200 repeats. Phosphorylated TDP-43 is present in the cytoplasm of iPS cell-derived motor neurons (iPSMNs) in *LRP12*-ALS, a finding that reproduces the pathological hallmark of ALS. RNA foci are more prominent in muscle and iPSMNs in *LRP12*-ALS than in *LRP12*-OPDM. Muscleblind-like 1 aggregates are observed only in OPDM muscle. In conclusion, CGG repeat expansions in *LRP12* cause ALS and OPDM, depending on the length of the repeat. Our findings provide insight into the repeat length-dependent switching of phenotypes.

Introduction

Amyotrophic lateral sclerosis (ALS [MIM: 105400]) is characterized clinically by muscle weakness and spasticity and pathologically by progressive loss of upper and lower motor neurons.[1] Progressive muscular atrophy (PMA) is a variant of ALS characterized by lower motor neuron disturbance. To date, more than 30 causative variants for ALS have been identified.[2] Repeat expansions in *ATXN2* (MIM: 601517)[3] and *C9orf72* (MIM: 614260)[4,5] are associated with ALS. In particular, GGGGCC repeat expansion in intron 1 of *C9orf72* is the most common cause in the European population.[4,5] The GGGGCC repeats in *C9orf72* are translated into aggregating dipeptide-repeat proteins, which can reduce ribosome levels,[6,7] in frontotemporal dementia/ALS. However, the molecular mechanisms by which repeat expansions cause ALS aren't fully known.

Oculopharyngeal distal myopathy (OPDM) is a muscular disorder characterized by ptosis, external ophthalmoplegia, and weakness of the pharyngeal and distal limb muscles. In 2019, CGG repeat expansion in *LRP12* was identified as a causative variant for OPDM[8] (OPDM1, *LRP12*-OPDM [MIM: 164310]), followed by the discovery of the repeat expansions in other genes, including *GIPC1* (OPDM2 [MIM: 618940]),[9] *NOTCH2NLC* (OPDM3 [MIM: 619473]),[10,11] and *RILPL1* (OPDM4 [MIM: 619790]).[12,13] Although abnormal RNA accumulation and translation of expanded CGG/GGC repeats are suspected to be the common disease mechanisms, the etiopathogenesis of OPDM isn't fully clear.

We report that CGG repeat expansion in *LRP12* is a cause of ALS. Differences in repeat lengths have different toxicities, leading to the different phenotypes.

Subjects and methods

Participants

We included two ALS-affected families and 1,039 individuals with ALS in the Hiroshima University cohort, 40 families with ALS in the Tohoku University cohort, 15 individuals with OPDM, and 853 healthy control participants. We obtained DNA samples

[1]Department of Molecular Epidemiology, Research Institute for Radiation Biology and Medicine, Hiroshima University, Hiroshima, Japan; [2]Department of Neurology, National Hospital Organization Kure Medical Center and Chugoku Cancer Center, Hiroshima, Japan; [3]Department of iPS Cell Applied Medicine, Graduate School of Medicine, Kansai Medical University, Osaka, Japan; [4]Department of Clinical Neuroscience and Therapeutics, Hiroshima University Graduate School of Biomedical and Health Sciences, Hiroshima, Japan; [5]Department of Genetics and Cell Biology, Research Institute for Radiation Biology and Medicine, Hiroshima University, Hiroshima, Japan; [6]Department of Neurology, Tohoku University Graduate School of Medicine, Miyagi, Japan; [7]Department of Medical Genetics, Tohoku University Graduate School of Medicine, Miyagi, Japan; [8]Department of Neuromuscular Research, National Institute of Neuroscience, National Centre of Neurology and Psychiatry, National Centre Hospital, Tokyo, Japan; [9]Institute of Medical Genetics, Tokyo Women's Medical University, Tokyo, Japan; [10]Department of Neurology, Wakayama Medical University, Wakayama, Japan; [11]Department of Neurology, Kansai Medical University, Osaka, Japan; [12]Department of Neuropathology, Institute for Medical Science of Aging, Aichi Medical University, Nagakute, Japan; [13]Department of Neurology, Tokushima University Graduate School of Biomedical Sciences, Tokushima, Japan
[14]Present address: Department of Medical Genetics, Tokushima University Graduate School of Biomedical Sciences, Tokushima, Japan
[15]Present address: Department of Molecular and Cellular Physiology, Graduate School of Medicine Yamaguchi University, Ube, Japan
[16]These authors contributed equally
*Correspondence: hkawakam@hiroshima-u.ac.jp
https://doi.org/10.1016/j.ajhg.2023.05.014.

from four individuals with ALS, one individual with OPDM, one neurologically healthy participant in family 1, and two affected individuals and three neurologically healthy participants in family 2. We also obtained muscle specimens from 14 individuals with ALS, 15 individuals with OPDM, and 5 negative controls (NCs). We performed histopathological examinations of muscle tissues from three individuals with ALS and three individuals with OPDM and compared these with those from five NCs (Table S1). Neurologists evaluated all participants with ALS and OPDM.

Approval was obtained from the ethics committee of Hiroshima University, Tohoku University, National Center of Neurology and Psychiatry, National Hospital Organization Kure Medical Center and Chugoku Cancer Center, and Aichi Medical University. All participants provided written informed consent. The procedures used in this study adhere to the tenets of the Declaration of Helsinki.

DNA, RNA, and protein extraction

Genomic DNA was extracted from leukocytes using QuickGene-610L (KURABO). DNA, RNA, and protein extractions from muscle tissues were performed using TRIzol Reagent (Invitrogen) according to the manufacturer's instructions. DNA and RNA concentrations were measured with a NanoDrop apparatus (Thermo Fisher Scientific), and protein concentration was determined with a BCA Protein Assay Kit (Pierce). RNA and protein samples were stored at −80°C, and DNA was stored at −4°C until use.

Homozygosity haplotype analysis and linkage analysis

We obtained SNP genotyping data using the GeneChip Human Mapping 500K Array Set (Affymetrix). Homozygosity haplotype analysis was performed with the HH analysis program (http://www.hhanalysis.com/),[14] and linkage analysis was conducted using Allegro (https://www.decode.com/software/allegro/).[15]

Short-read sequencing

We performed exome and whole-genome sequencing using the Illumina platform sequencer. The data were analyzed as previously described,[16] apart from the use of hg38 for genomic coordinates. The identified variants were filtered by following criteria: (1) two of more prediction algorithms (SIFT[17] [https://sift.bii.a-star.edu.sg/index.html], PolyPhen-2[18] [http://genetics.bwh.harvard.edu/pph2/], and CADD[19] [https://cadd.gs.washington.edu/]) were positive (the CADD score threshold was set to >15) and (2) the frequency in the gnomAD database (https://gnomad.broadinstitute.org/) was ≤0.001.

Long-read sequencing

Library preparation was performed using a ligation sequencing kit (SQK-LSK-109, Oxford Nanopore Technologies) in accordance with the manufacturer's protocol. Sequencing was conducted using a MinION and R9.4.1 flow cell (Oxford Nanopore Technologies). We used Guppy (v.3.2.2, https://community.nanoporetech.com) for base calling, LAST (v.983, https://github.com/mcfrith/last-genome-alignments) for mapping, and tandem-genotypes[20] for the evaluation of repeat expansion. Methylation analysis was performed using Guppy and Nanopolish (v.0.11.2, https://github.com/jts/nanopolish/blob/master/docs/source/index.rst). Methylation status was visualized with methplotlib[21] (v.0.7.0, https://github.com/wdecoster/methplotlib) and the graph was inverted manually to adjust to the transcript direction.

Repeat-primed PCR analysis and fluorescence amplicon length analysis PCR

Repeat-primed PCR and fluorescence amplicon length analysis PCR were performed as described in a previous report.[8] To prepare the sample for electrophoresis, we mixed 1 μL of PCR product, 0.25 μL of GeneScan 500 ROX Size Standard, and 11.75 μL of Hi-Di Formamide. The samples were incubated at 95°C for 5 min. We used the ABI 3130 Genetic Analyzer for electrophoresis and Peak Scanner software (Thermo Fisher Scientific) for fragment size analysis.

Cas9-mediated enrichment and nanopore sequencing

The CGG repeat region in *LRP12* was enriched using the CRISPR-Cas9 system according to the protocol provided by Oxford Nanopore Technologies. We used two crRNAs (5′-CAAGGCGACAG CUAUUUCUCGUUUUAGAGCUAUGCU-3′ and 5′-UUGACUACU UGGUACAAUGGGUUUUAGAGCUAUGCU-3′) for the regions approximately 2,000 base pairs away from the repeat.

Generation and maintenance of human iPSCs

The use of human induced pluripotent stem cells (hiPSCs) was approved by the ethics committees of the RIKEN Center for Developmental Biology and Kansai Medical University. For the generation of hiPSCs from six affected individuals and one healthy volunteer, *OTX2*, *SOX2*, *KLF4*, *L-MYC*, *LIN28*, *EBNA1*, and p53 carboxy-terminal dominant-negative fragments were transduced into peripheral blood mononuclear cells using episomal vectors as previously described[22,23] (see also Table S2). All participants provided written informed consent. The healthy subject-derived iPSC lines 201B7 and HC6[24,25] were used as the controls. The hiPSCs were maintained on laminin (iMatrix-511; Nippi) in StemFit AK02N (Ajinomoto) at 37°C in a 5% CO_2 incubator, according to the manufacturer's instructions. Passages were performed every seventh day. Prior to passaging, the culture dishes were coated with iMatrix-511 in PBS. The hiPSC colonies were treated with 0.5× TrypLE Express Enzyme (Thermo Fisher Scientific) and dissociated into single cells by gentle pipetting. The dissociated hiPSCs were suspended in StemFit AK02N, plated at a density of 1,350 cells/cm^2, and cultured in StemFit AK02N with a 10 μM Y-27632 ROCK inhibitor (TOCRIS, Nacalai Tesque). The medium was changed to StemFit AK02N without Y-27632 on the following day and then changed every other day.

Spinal MN differentiation from human iPSCs

To generate stable and inducible iPSC lines for the differentiation of spinal motor neurons (MNs), the iPSCs were transfected with epB-Bsd-TT-NIL, an enhanced piggyBac transposable inducible expression vector[26] containing the *Ngn2*, *Isl1*, and *Lhx3* transgenes.[27] MN differentiation from iPSCs was performed as described previously,[28,29] with a slight modification. Briefly, the iPSCs were dissociated to single cells with 0.5× TrypLE Express and plated in StemFit AK02N with 10 μM Y-27632 on 1% Matrigel (Corning) at a density of 1×10^5 cells/cm^2. The following day, differentiation was induced by adding 1 μg/mL doxycycline (Sigma-Aldrich) in DMEM/F-12 GlutaMAX (Thermo Fisher Scientific). The medium was changed every day. After 48 h of doxycycline induction, the medium was changed to Neurobasal/B27 (Neurobasal Medium supplemented with 1× B27 supplement, 1× GlutaMAX, and 0.5× penicillin/streptomycin [Thermo Fisher Scientific]) containing 1× non-essential amino acids (Thermo Fisher Scientific), 5 μM DAPT (Sigma-Aldrich), and 4 μM SU5402 (Calbiochem). On day 5, the

cells were dissociated with Accutase (Thermo Fisher Scientific) or 1× TrypLE Express and plated onto poly-D-lysine (Sigma-Aldrich)/laminin (Thermo Fisher Scientific)-coated culture dishes or eight-well culture slides (Corning) at a density of 1×10^5 cells/cm^2 in Neurobasal/B27 containing 10 μM Y-27632. After overnight incubation, on day 6, the medium was changed to Neurobasal/B27 supplemented with 20 ng/mL BDNF and 10 ng/mL GDNF (both from R&D Systems). Half of the medium was replaced with a fresh medium every 3–4 days.

Quantitative PCR

RNA (400 ng) was reverse-transcribed into cDNA using RevTra Ace reverse transcriptase and $Oligo(dT)_{20}$ Primer (TOYOBO). Quantitative PCR was performed using THUNDERBIRD SYBR qPCR Mix (TOYOBO) and the StepOnePlus system (Thermo Fisher Scientific) with the following primers: *LRP12* (forward: 5′-GCCTCAT CTGTGGCCTGTTA-3′; reverse: 5′-ACGAGGGAGGAGCTTCTCTT CCCTCGT-3′) and *GAPDH* (forward: 5′-GAAGGTGAAGGTCGG AGTCAAC-3′; reverse: 5′-CAGAGTTAAAAGCAGCCCTGGT-3′). We performed triplicate PCR reactions and used the $2^{-\Delta\Delta Ct}$ method to evaluate relative expression.

ELISA

ELISA was performed using the LRP12 ELISA Kit (MyBioSource) according to the provided protocol. Optical density was measured with Varioskan Flash (Thermo Fisher Scientific). The LRP12 values were normalized to the total protein amount.

Immunocytochemistry

Immunocytochemistry was performed as previously reported[30,31] using the primary antibodies described in Table S4. Nuclear counterstaining was performed with DAPI (Nacalai Tesque). Images were acquired using a confocal microscope (LSM710, Carl Zeiss). In addition, we created cell blocks of iPSMNs. The cell blocks were prepared using HistoGel (Richard-Allan Scientific) according to the manufacturer's instructions. Briefly, the cell pellets were fixed with 10% neutral buffered formalin for at least 2 h, followed by centrifugation. After decanting, a few drops of warm HistoGel were added to the cell pellet, gently mixed, and immediately centrifuged. After a few hours in a refrigerator, solid HistoGel buttons containing the cells were transferred to a tissue cassette and embedded in paraffin according to the standard procedure for small biopsies in a Tissue-Tek REC6 tissue processor (Sakura Finetek).

For each specimen of the iPSMN cell blocks, 8 μm transverse sections were subjected to immunocytochemical or immunofluorescence detection after the cell blocks were assessed as empty, scant, moderate, or highly cellular on the basis of the cellularity of the HE-stained section. For immunocytochemical analysis, the sections were immunostained using a Ventana BenchMark GX automated slide staining system (Ventana Medical Systems) with a mouse monoclonal pTDP43 antibody (Table S4). For immunofluorescence analysis, the sections were incubated with primary mouse and rabbit antibodies overnight at 4°C after washing in PBS and thereafter directly visualized using an anti-mouse secondary antibody conjugated with Alexa Fluor 568 and an anti-rabbit secondary antibody conjugated with Alexa Fluor 488. The primary antibodies consisted of mouse monoclonal antibodies against MBNL1 and rabbit polyclonal antibodies against LRP12 (Table S4). The sections were photographed using a BIOREVO BZ-9000 fluorescence microscope (Keyence).

Immunohistochemical analysis

All muscle biopsies were performed for diagnostic purposes. Muscle biopsy specimens were frozen in liquid nitrogen-cooled isopentane. For each specimen of muscle tissues, 8 μm transverse sections were subjected to immunohistochemical and immunofluorescence detection. For immunohistochemical analysis, the sections were immunostained using a Ventana BenchMark GX automated slide staining system (Ventana Medical Systems) with a mouse monoclonal pTDP43 antibody (Table S4). For immunofluorescence analysis, the sections were incubated with primary mouse and rabbit antibodies overnight at 4°C after washing in PBS and then directly visualized using an anti-mouse secondary antibody conjugated with Alexa Fluor 568 and an anti-rabbit secondary antibody conjugated with Alexa Fluor 488. The primary antibodies consisted of mouse monoclonal antibodies against MBNL1 and rabbit polyclonal antibodies against LRP12. The sections were photographed using a BIOREVO BZ-9000 fluorescence microscope (Keyence).

Florescence *in situ* hybridization

The iPSMN cells were fixed in 4% paraformaldehyde for 10 min, permeabilized in 70% ethanol on ice, equilibrated in 50% formamide/2× SSC for 30 min at 66°C, hybridized for 3 h at 72°C with denatured nucleic acid probe (50 nM), and pre-heated at 80°C for 10 min in hybridization buffer (Sigma-Aldrich). The cells were washed twice with 50% formamide/2× SSC for 20 min at 72°C and twice with 2× SSC at room temperature. To combine FISH with immunofluorescence staining, after being washed with 2× SSC, the cells were washed with PBS and blocked with 10% normal donkey serum in PBS/0.05% Tween 20 for 20 min at room temperature. The cells were then incubated with primary antibodies in PBS/0.05% Tween 20 at 4°C. The following primary antibodies were used: Tubulin β3 (TUBB3) and LRP12. After three rinses with PBS/0.05% Tween 20, the cells were incubated with the appropriate secondary antibodies containing DAPI for 1 h at room temperature. The following secondary antibodies were used: Cy5-conjugated donkey anti-mouse IgG and Alexa Fluor 488-conjugated donkey anti-rabbit IgG (both from Jackson Immunoresearch). After three rinses with PBS, the cells were mounted with SlowFade Gold (Thermo Fisher Scientific). Images were acquired with an LSM710 microscope.

For the iPSMN cell and muscle tissue blocks, 8 μm sections were permeabilized and equilibrated on a VP 2000 automated processor (Abbott Molecular) according to the manufacturer's protocol. The sections were hybridized for 3 h at 72°C with a denatured nucleic acid probe (50 nM) and then washed twice with 50% formamide/2 × SSC for 20 min at 72°C and twice with 2 × SSC at room temperature. To combine FISH with immunofluorescence staining, after washing with 2 × SSC and PBS, the sections were incubated with primary mouse and rabbit antibodies overnight at 4°C after washing in PBS and afterward directly visualized using an anti-mouse secondary antibody conjugated with Alexa Fluor 568 and an anti-rabbit secondary antibody conjugated with Alexa Fluor 488. Images were acquired using a BIOREVO BZ-9000 fluorescence microscope (Keyence).

Statistics

All statistical analyses were performed with R software (v.4.0.3) or Prism 8 software (GraphPad Software). Differences were considered statistically significant if the p value was less than 0.05. We performed Steel's test for qPCR and ELISA experiments using R software and Mann-Whitney U and Kruskal-Wallis tests for immunofluorescence and FISH analysis using Prism 8 software.

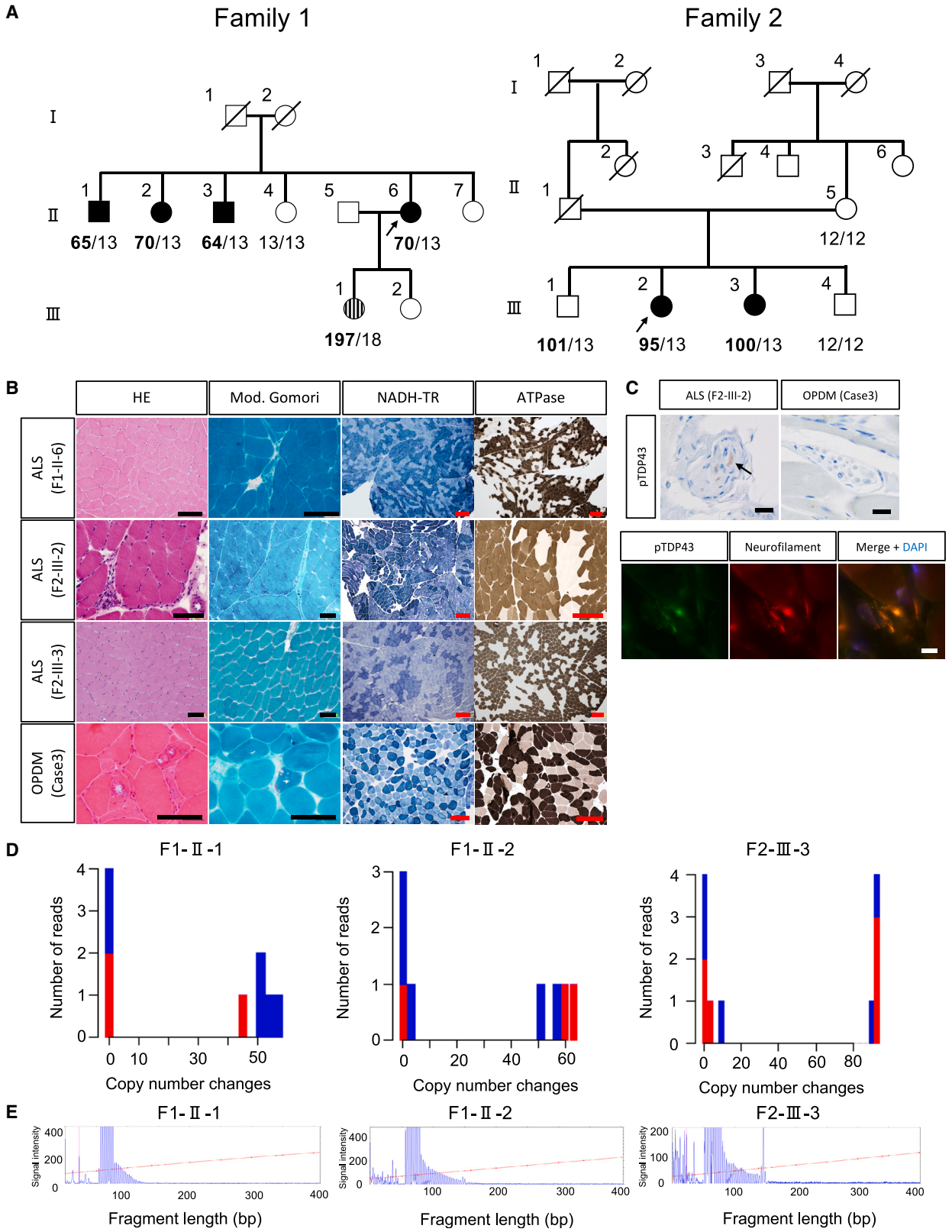

Figure 1. Genetic analysis and pathological characteristics of ALS-affected families

(A) Pedigree chart of the families with ALS. The arrows indicate the probands. The black, striped, and white symbols indicate ALS-affected, OPDM-affected, and unaffected participants, respectively. Indicated below the symbols is the number of CGG repeats in *LRP12* (bold letters indicate an expansion of the repeat).

(B) Muscle biopsy specimens of three participants did not show any myopathic findings including rimmed vacuoles by hematoxylin and eosin (HE) and modified Gomori trichrome (Mod. Gomori) staining. However, muscle tissues of three participants presented fiber type

(legend continued on next page)

Results

Initially, we analyzed six individuals with ALS, one individual with OPDM, and four unaffected individuals from two Japanese ALS-affected families (Figure 1A). At the time of genetic analysis, the individual with OPDM (F1-III-1) had not been diagnosed with OPDM because of minor symptoms. However, she was treated as an affected individual because she had myalgia, similar to her mother (F1-II-6). All affected individuals presented with slowly progressing muscle weakness beginning in their 40s. In their 50s, they showed muscle weakness, and two had a positive jaw reflex. Radiological abnormalities were not observed, except for atrophy of the thigh muscles. Electromyography showed active and chronic denervation in the cervical and lumbosacral regions. In their 60s, the individuals started to use wheelchairs. Muscle biopsies were performed for three participants (F1-II-6, F2-III-2, and F2-III-3) to exclude myopathy because of the high levels of serum creatinine kinase. Muscle biopsy specimens of three participants did not show any myopathic findings including rimmed vacuoles, a pathological hallmark of autophagic vacuolar myopathies including OPDM by hematoxylin and eosin (HE), and modified Gomori trichrome (mGT) staining (Figure 1B). However, muscle tissues of three participants presented fiber type grouping by NADH-tetrazolium reductase (NADH-TR) and ATPase staining and those of F1-II-6 and F2-III-2 presented grouped atrophy by HE and mGT staining. These two findings suggested neuropathy or motor neuron disease but not muscle disease, such as *LRP12*-OPDM (Figure 1B). In addition, the muscle biopsy specimen of F2-III-2 included intramuscular nerve bundles, which showed an axonal phosphorylated TAR DNA-binding protein of 43 kDa (pTDP-43) accumulation (Figure 1C) but no accumulations of fused in sarcoma (FUS), SQSTM1/p62, and ubiquitin (Figure S1), similar to the pathological findings in the muscle tissues of individuals with simplex ALS in our previous study.[32] These individuals were all clinically diagnosed with ALS according to the revised El Escorial and Awaji diagnostic criteria.[33,34] A summary of the data on the study participants is given in Table S2 and supplemental note.

To identify the causative variant, SNP genotyping was first performed. Because homozygosity haplotype analysis identified the shared haplotypes in the affected participants (F1-II-1, F1-II-2, F1-II-3, F1-II-6, F1-III-1, F2-III-2, and F2-III-3), two families were considered to have a common causative variant (Figure S2A). Linkage analysis using Allegro[15] identified several regions with LOD scores of ~2 (Figure S2B). Next, we performed exome sequencing in the affected individuals (F1-II-6, F1-III-1, F2-III-2, and F2-III-3), as well as whole-genome sequencing (in F1-II-1, F1-II-2, and F2-III-3), with a short-read sequencer and could not identify candidate variants. We used a long-read sequencer for the affected individuals (F1-II-1, F1-II-2, and F2-III-3). Using tandem-genotypes,[20] we identified CGG repeat expansion in the 5'-untranslated region (UTR) of *LRP12* (GenBank: NM_013437.5, chr8:104,588,961–104,588,999; hg38) in these three individuals (Figure 1D). This repeat expansion was validated using repeat-primed PCR (Figure 1E) and fluorescence amplicon length analysis. We confirmed the repeat expansion in all affected individuals (F1-II-1, F1-II-2, F1-II-3, F1-II-6, F1-III-1, F2-III-2, and F2-III-3). One unaffected participant (F2-III-1) also had this variant. Although he has reached a sufficient age for *LRP12*-ALS onset (57 years), we speculate that this is an example of incomplete penetrance.[8] One individual (F1-III-1) developed mild muscle weakness of the extremities, unilateral facial muscle weakness, and dysphagia after analysis and was diagnosed with *LRP12*-OPDM at age 44.

We also screened a cohort with familial motor neuron disease at Tohoku University (40 families) and identified two PMA-affected families with repeat expansion in *LRP12* (Figures 2A and 2B). In addition, we screened the ALS-affected individuals and healthy control (HC) participants in our cohort for the repeat expansion in *LRP12*. Fluorescence amplicon length analysis and repeat-primed PCR revealed the repeat expansion in 3 of 1,039 participants with ALS. In comparison, each of the 853 HC participants had no more than 50 repeats (Figure 2D). One of the three individuals had familial PMA (Figure 2C). Although one of the two simplex individuals was clinically diagnosed with PMA (simplex individual 1), the other individual had typical ALS (simplex individual 2) and underwent tracheostomy for respiratory failure 4 years after onset. All participants with ALS and PMA had fewer than 100 repeats. These results demonstrate that CGG repeat expansions in *LRP12* cause both familial and simplex ALS, as well as PMA.

Next, we performed Cas9-mediated target sequencing to evaluate the CGG repeat and methylation status of the CpG island in *LRP12*. We determined that the repeat

grouping by NADH-tetrazolium reductase (NADH-TR) and ATPase staining and those of F1-II-6 and F2-III-2 presented grouped atrophy by HE and mGT staining. By contrast, the OPDM-affected individuals showed myopathic changes, including rimmed vacuoles, but no neuropathic changes.
(C) Immunohistochemistry revealed axonal phosphorylated TDP-43 (pTDP-43)-positive accumulations in intramuscular nerve bundles (arrow), which were not observed in the OPDM-affected individuals. Immunofluorescence analysis showed that pTDP-43 was colocalized with the neurofilament in intramuscular nerve bundles.
(D) CGG repeat length in *LRP12* analyzed by nanopore sequencing in F1-II-1, F1-II-2, and F2-III-3. The x axis indicates copy number changes relative to the reference human genome, and the y axis indicates the number of reads. The red bar indicates the number of forward-strand reads, and the blue bar indicates the reverse-strand reads.
(E) Repeat-primed PCR for F1-II-1, F1-II-2, and F2-III-3.
Scale bars: (B) black, 100 μm; red, 200 μm; (C) bright-field, 20 μm, immunofluorescence, 10 μm.

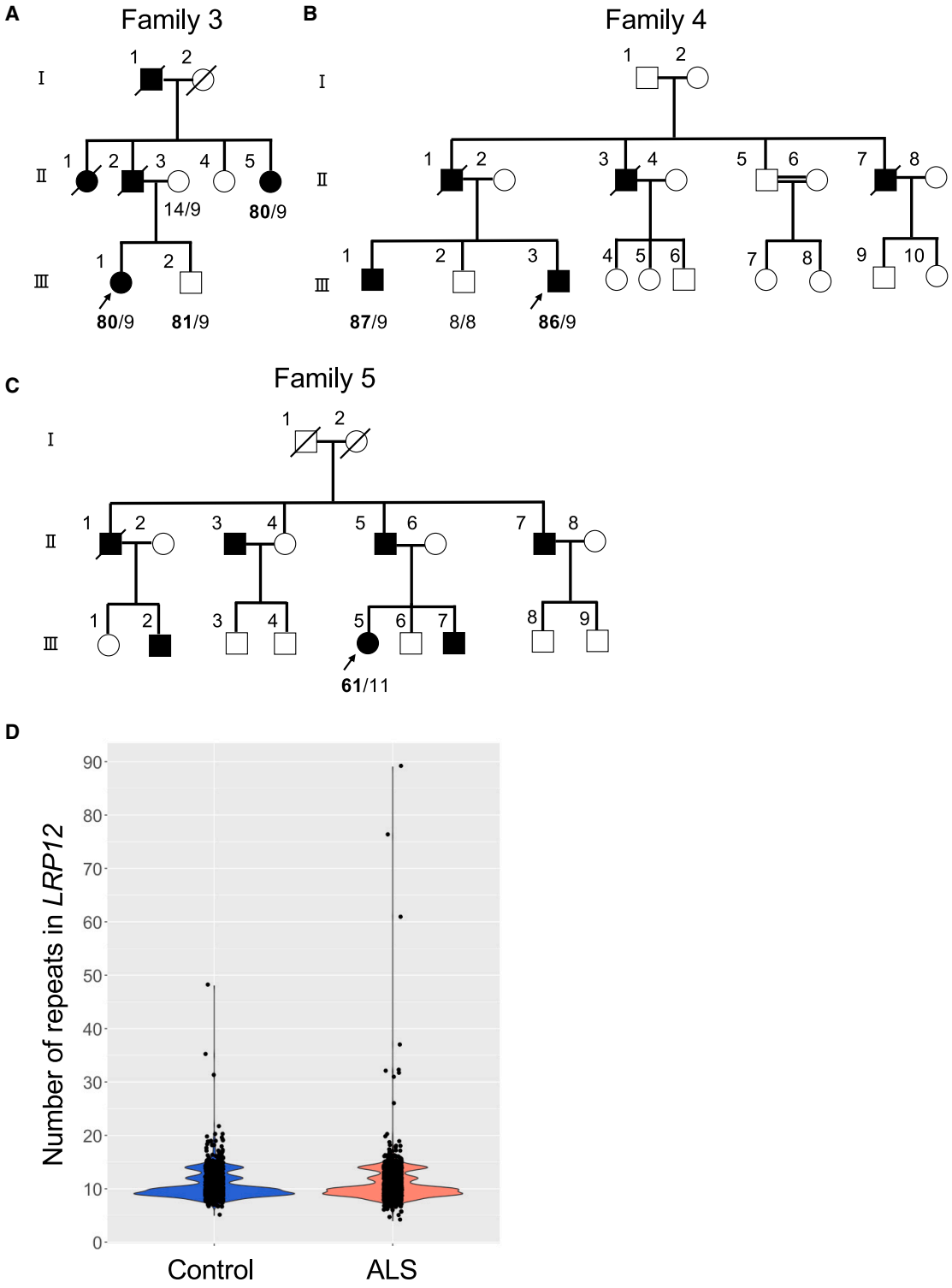

Figure 2. Additional families and distribution of CGG repeat length in *LRP12*

(A–C) Pedigree chart of the families with PMA. The arrows indicate the probands. The black and white symbols indicate affected and unaffected participants, respectively. The numbers below the participants are the CGG repeat numbers in *LRP12* (bold letters indicate an expansion of the repeat).

(D) Number of CGG repeats in control participants (n = 853) and in participants with ALS (n = 1,039). Three out of 1,039 ALS-affected individuals demonstrated CGG repeats longer than 50, whereas all control participants had repeat counts shorter than 50.

length in the affected participants was from 64 to 70 in family 1 and approximately 95 and 100 in family 2 (Figure S3). However, the OPDM-affected individual (F1-III-1) had a longer expansion (197 repeats) than the other participants in family 1 (Figure 1A, see Figure S3 for full variant descriptions). Methylation analysis revealed that

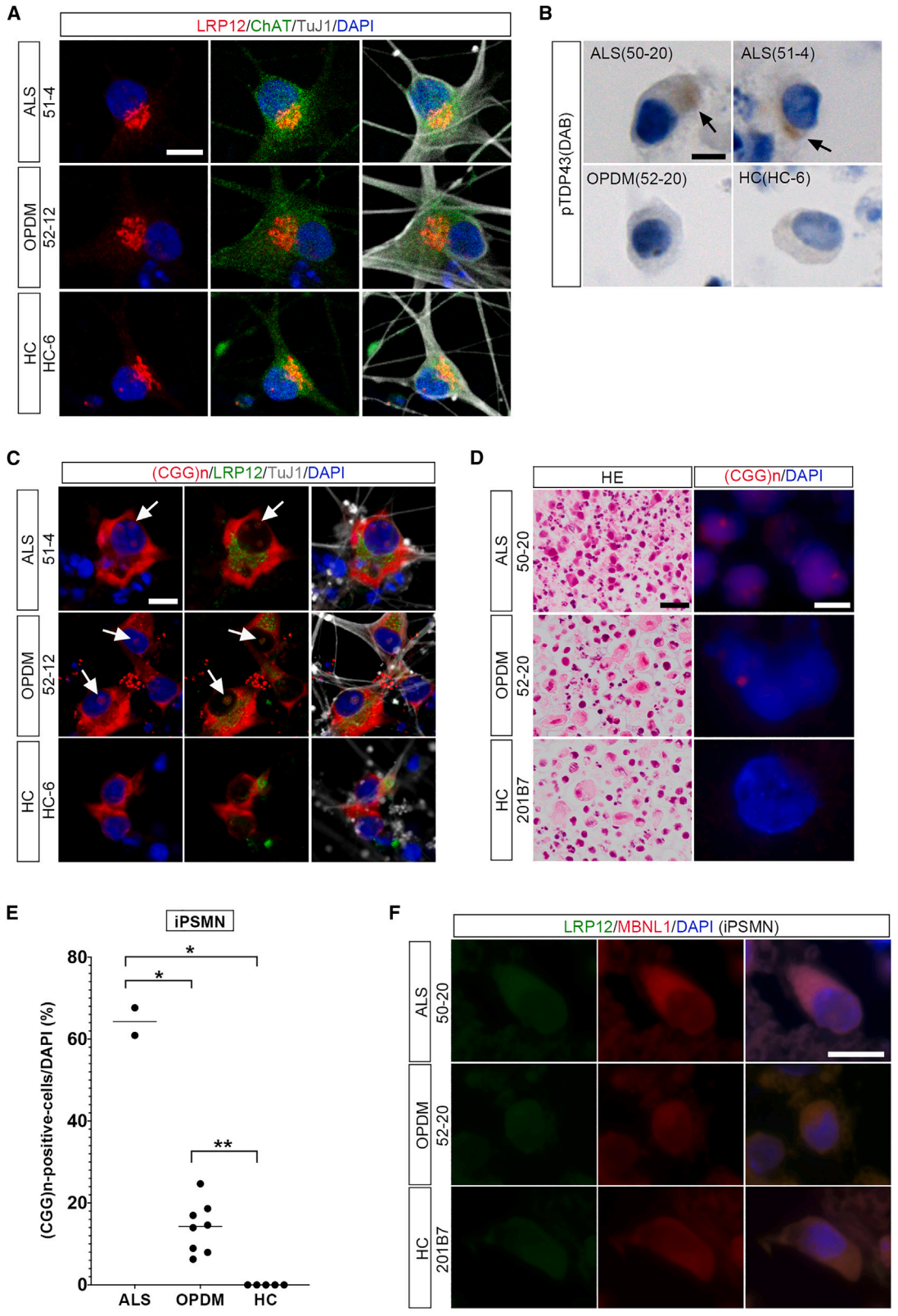

Figure 3. Cytopathological characteristics of iPS cell-derived spinal motor neurons (iPSMNs)
(A) iPSMNs showing cytoplasmic and nuclear staining for LRP12 in *LRP12*-ALS-affected and *LRP12*-OPDM-affected individuals.
(B) iPSMNs from *LRP12*-ALS-affected individuals showed accumulations of pTDP-43 in the cytoplasm.
(C) FISH showing $(CGG)_n$-positive accumulations in the nuclei of iPSMNs from *LRP12*-ALS-affected and *LRP12*-OPDM-affected individuals. These aggregates colocalized with LRP12 (white arrows). HCs did not show any signals.
(D) Cell blocks of iPSC-derived neurons from *LRP12*-ALS-affected and *LRP12*-OPDM-affected individuals showing intranuclear RNA accumulations, although HE staining did not show abnormality. HCs did not show any nuclear signals.

(legend continued on next page)

the frequency of 5-methylcytosine in the lower region of the repeat was increased in two participants (F1-III-1 and F2-III-1) compared with the other participants (Figure S4). F2-III-1, with 101 repeats, may go on to develop ALS or OPDM but was currently asymptomatic. These results suggest that phenotypic differences may be caused by differences in repeat lengths and that methylation might decrease *LRP12* mRNA expression, further modifying the phenotype.

To evaluate the impact of methylation status on *LRP12* mRNA expression and clarify the pathogenetic differences between ALS and OPDM, we compared the skeletal muscle tissues of *LRP12*-ALS-affected participants (F1-II-6, F2-III-2, and F2-III-3) with those from simplex ALS-affected individuals (n = 12), *LRP12*-OPDM-affected individuals (n = 15), and negative controls (NC) (n = 7) at Hiroshima University, Tohoku University, and the National Center for Neurology and Psychiatry. We first quantified muscular *LRP12* mRNA using quantitative PCR (qPCR). In the *LRP12*-OPDM group, *LRP12* mRNA was increased in some individuals, but *LRP12* mRNA was not significantly different compared to control group. By contrast, *LRP12* mRNA in the *LRP12*-ALS group was increased significantly (Figure S5A). However, significant changes in LRP12 levels were not observed in the muscle (Figure S5B).

Based on the *LRP12* mRNA and protein results, we analyzed the cytopathological features of iPSMNs from two *LRP12*-ALS-affected individuals (F1-II-6 and F2-III-2) and compared these with those from *LRP12*-OPDM-affected individuals and HC individuals (Table S3). Immunofluorescent analysis revealed LRP12-positive intranuclear and cytoplasmic inclusions in the iPSMNs of individuals with *LRP12*-ALS and OPDM. iPSMNs from HCs showed LRP12-positive inclusions in the cytoplasm but not in the nuclei (Figure 3A). In addition, iPSMNs from *LRP12*-ALS-affected individuals had cytoplasmic granules positive for pTDP-43 (Figure 3B), which pathologically characterizes the vast majority of ALS-affected individuals.[1,35,36] These granules did not appear skein like or round but were similar to the mislocalized inclusions seen in iPSCs derived from ALS-affected individuals in a previous report.[37] iPSMNs from *LRP12*-OPDM-affected individuals and HCs did not contain pTDP-43-positive cytoplasmic granules (Figures 3B and S6A). These pathological findings suggest that *LRP12*-ALS is part of the ALS spectrum with TDP-43 pathology.

To examine whether the length of the CGG repeat affected inclusion formation in iPSMNs and muscle tissues, we performed RNA fluorescence *in situ* hybridization (RNA-FISH). A summary of the OPDM-affected individuals and NC individuals for whom muscle biopsy specimens were obtained is given in Table S1. RNA-FISH revealed nuclear RNA accumulations in iPSMNs from both *LRP12*-ALS-affected and *LRP12*-OPDM-affectged individuals but not HCs. Intranuclear RNA accumulations were colocalized with LRP12 (Figure 3C). The cytoplasm of iPSMNs from all affected individuals and HCs showed non-specific findings associated with the fixation process. We also examined paraffin-embedded iPSMN cell blocks to detect nuclear RNA accumulations. These iPSMN specimens showed intranuclear RNA accumulations in both *LRP12*-ALS-affected individuals and *LRP12*-OPDM-affected individuals. Cell blocks from HCs did not show nuclear RNA accumulations (Figures 3D and S6B). The iPSMNs of individuals with *LRP12*-ALS frequently showed nuclear RNA accumulations (64.3 ± 4.8/100 nuclei [mean ± SD]) compared with those of individuals with *LRP12*-OPDM (14.0 ± 6.2/100 nuclei) ($p = 0.044$) (Figures 3E and S6C). iPSMNs from *LRP12*-OPDM-affected individuals showed nuclear RNA accumulations more frequently than those from HCs ($p < 0.01$). In addition, RNA-FISH showed nuclear RNA accumulations in the muscle biopsy specimens of both *LRP12*-ALS-affected and *LRP12*-OPDM-affected individuals but not NCs (Figures 4A and S7). Approximately 10% of the intranuclear RNA accumulations were colocalized with LRP12 in the *LRP12*-ALS and *LRP12*-OPDM muscle specimens. The frequency of nuclear RNA accumulations in muscle tissues from *LRP12*-ALS-affected individuals (27.3 ± 4.8/100 nuclei [mean ± SD]) was not significantly higher than that in muscle from *LRP12*-OPDM-affected individuals (11.7 ± 1.2/100 nuclei) ($p = 0.10$) (Figure 4B). These findings suggest that RNA accumulations are associated with the pathogenesis of *LRP12*-ALS.

We observed an association between LRP12 and muscleblind-like 1 (MBNL1). MBNL1 binds specifically to expanded CGG repeats in RNA,[38] and MBNL1 sequestration causes dysregulation of mRNA splicing. MBNL1 was not detected in the nuclei of paraffin-embedded cell blocks of iPSMNs from *LRP12*-ALS-affected or *LRP12*-OPDM-affected individuals or HCs (Figures 3F and S8A). MBNL1 was not detected in the nuclei of muscle tissues from *LRP12*-ALS-affected individuals or control individuals but colocalized with LRP12-positive intranuclear inclusions in muscle tissues from *LRP12*-OPDM-affected individuals (Figures 4C and S8B). Given that the muscles in OPDM3[11] and OPDM4,[12,13] which have the same 5'-UTR CGG repeat expansion, were positive for MBNL1 aggregates, MBNL1 dysfunction in muscles may be necessary for the development of muscle atrophy.

(E) Dots represent experimental trials. Number of individuals is two in ALS group, four in OPDM group, and three in HC group. FISH revealed that nuclear $(CGG)_n$-positive accumulations were more frequent in the nuclei of individuals with *LRP12*-ALS than in the nuclei of individuals with *LRP12*-OPDM ($p = 0.044$).
(F) Immunofluorescence analysis showed that MBNL1 was not localized in the nuclei of paraffin-embedded cell blocks of iPSMNs from individuals with *LRP12*-ALS or *LRP12*-OPDM, or HCs.
Scale bars: (A)–(C), 10 μm; (D) HE, 20 μm, immunofluorescence, 5 μm; (F) 10 μm; *$p < 0.05$, **$p < 0.01$.

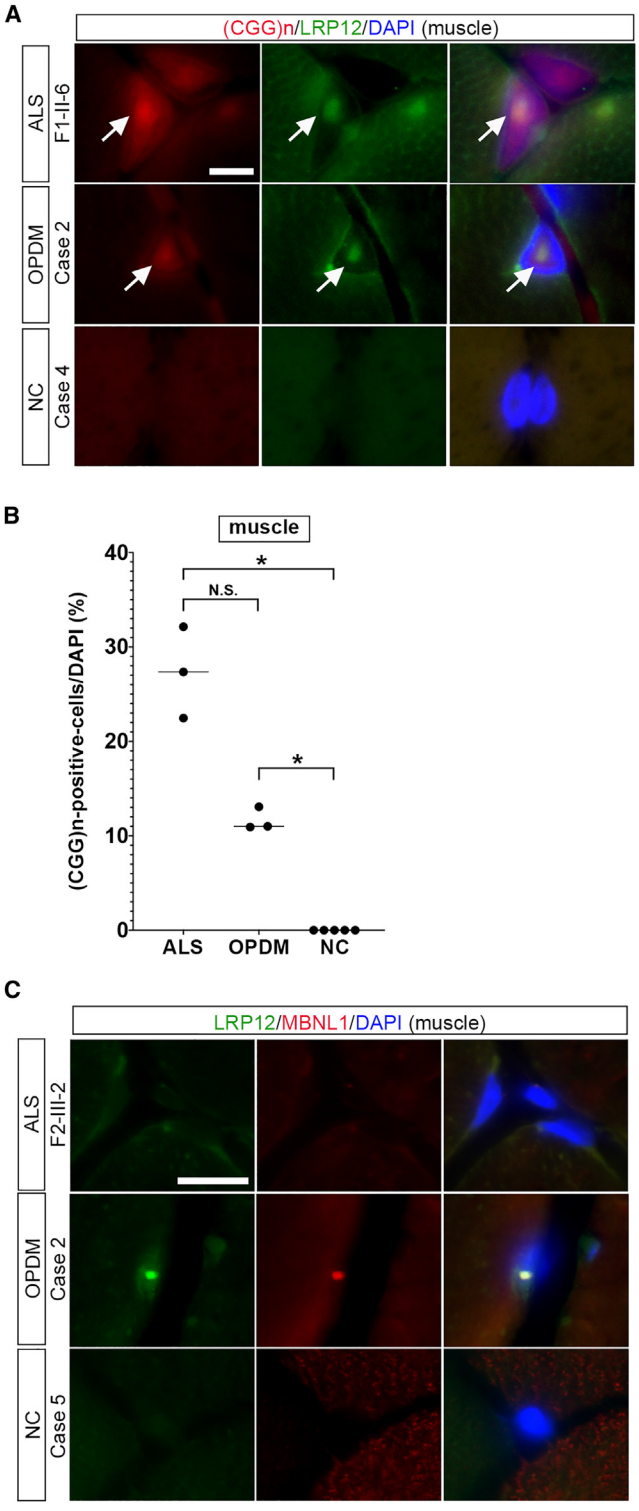

Figure 4. Pathological characteristics of muscles

(A) Intranuclear RNA accumulations in the muscles of individuals with *LRP12*-ALS and *LRP12*-OPDM, although HE staining did not show any abnormalities. HCs did not show any nuclear signals.

(B) Dots represent the individuals examined. The frequency of nuclear RNA accumulations in muscle tissues was not significantly higher in *LRP12*-ALS-affected individuals compared with that in *LRP12*-OPDM-affected individuals ($p = 0.10$).

(C) MBNL1 localization was not observed in the nuclei of the muscle tissues of *LRP12*-ALS-affected individuals or control individuals but was colocalized with *LRP12*-positive intranuclear inclusions in *LRP12*-OPDM-affected individuals.

Scale bars: (A) 5 μm; (C) 10 μm; *$p < 0.05$.

Discussion

We identified CGG repeat expansions in *LRP12* in two ALS-affected families, three PMA-affected families, and two simplex ALS-affected individuals. These individuals progressed more slowly than typical ALS-affected individuals and presented with lower motor neuron-dominant impairment. The repeat lengths in ALS-affected individuals are 64–100, shorter than those in OPDM-affected individuals, who have more than 100 repeats.[39] *LRP12* mRNA in muscle tended to be increased in *LRP12*-ALS compared with that in *LRP12*-OPDM-affected individuals and NCs, although the amount of LRP12 was not different. Intranuclear RNA accumulations were more prominent in iPSMNs from *LRP12*-ALS-affected individuals compared with those from *LRP12*-OPDM-affected individuals. Furthermore, iPSMNs from *LRP12*-ALS-affected and *LRP12*-OPDM-affected individuals did not have intranuclear MBNL1 aggregates that were observed in the muscles from *LRP12*-OPDM-affected individuals. Differences in toxic RNA levels and MBNL1 dysfunction, which may be repeat length dependent, might therefore underlie the observed phenotypic differences.

Repeat length-dependent phenotypic switching is known for the CGG repeat in the 5'-UTR of *FMR1* (MIM: 309550), which causes fragile X syndrome (FXS [MIM: 300624])[40] and fragile X-associated tremor/ataxia syndrome (FXTAS [MIM: 300623]).[41] The main cause of FXS is the suppression of *FMR1* expression caused by repeat-induced DNA methylation, while the pathophysiology of FXTAS involves RNA toxicity and repeat-associated non-AUG (RAN) proteins.[42–44] In contrast to *FMR1*, both *LRP12*-ALS and OPDM are caused by toxic gain-of-function mechanisms. We posit that repeat length-dependent gene expression changes and differences in MBNL1 aggregations play a critical role in the pathogenetic differences between ALS and OPDM. The repeat length in individuals with *LRP12*-ALS is shorter than 100, although almost all individuals with *LRP12*-OPDM have more than 100 repeats.[39] Even though motor neurons, not muscles, are thought to be the primary site of disease in ALS, the change in *LRP12* expression is greater in the muscle in *LRP12*-ALS-affected individuals than in *LRP12*-OPDM-affected individuals. However, further confirmation of this is needed due to the small sample size and large variance in the data. Consistent with this, nuclear RNA inclusions in muscle and iPSMNs are more prominent in *LRP12*-ALS than in *LRP12*-OPDM. These findings suggest that the amount of toxic RNA in the nucleus plays an important role in the pathogenesis of *LRP12*-ALS. We speculate that, as in the case of *C9orf72*, the aberrant RNA may promote the formation of stress granules and production of repeat-associated non-AUG (RAN) protein and cause TDP-43 aggregation, leading motor neuron death.[45]

Furthermore, MBNL1 dysfunction may play a more important role in OPDM. The aggregation of MBNL1 in the nucleus is not observed in *LRP12*-ALS but is found in *LRP12*-OPDM and other OPDMs, and it is associated with *NOTCH2NLC*[11] and *RILPL1*.[12] These and the clinical findings suggest that repeat expansions of more than 100 are needed for MBNL1 aggregation, so *LRP12*-ALS-affected individuals do not develop OPDM.

On the other hand, *LRP12*-ALS and *LRP12*-OPDM arise from differences in repeats in the same gene, and even *LRP12*-OPDM has been reported to have p63-positive inclusion bodies in neurons,[46] it may be possible that both diseases belong to a single spectrum. Further accumulation of autopsy reports is needed to be clear.

One limitation of this study is that we did not show the accumulation of RAN proteins. CGG repeats can be translated into polyglycine, polyarginine, and polyalanine proteins in the direction of the sense strand. Since polyarginine protein can be followed by normal LRP12 and detected by anti-LRP12 antibody, the LRP12 colocalized with CGG repeat RNA (Figures 3C and 4A) may be polyarginine protein. To confirm this, we need to analyze RAN proteins in the future.

In conclusion, we report that CGG repeat expansions in the 5'-UTR of *LRP12* cause ALS via a toxic gain-of-function mechanism. Differences in the levels of toxic RNA and MBNL1 dysfunction, in turn dependent on repeat length, may determine whether the affected individual develops ALS or OPDM.

Data and code availability

The genotyping microarray data and the sequence data obtained using massively parallel sequencing analysis and nanopore sequencing analysis, including whole-genome sequencing and exome sequencing, are available on request from the corresponding author. Because microarray data and whole-genome and exome sequence data are protected by the Personal Information Protection Law, these data are available under regulation by the institutional review board.

Supplemental information

Supplemental information can be found online at https://doi.org/10.1016/j.ajhg.2023.05.014.

Acknowledgments

This work was supported by JSPS KAKENHI (JP20K16580, 18H02535, 19K22983, and 21H04818), the Taiju Life Social Welfare Foundation, Takeda Science Foundation, Tsuchiya Memorial Medical Foundation, Uehara Memorial Foundation, the Serika Fund, the SENSHIN Medical Research Foundation, and Novartis Foundation for the Promotion of Science. We acknowledge the assistance of Dr. Alessandro Rosa, who provided the plasmid epB-Bsd-TT-NIL. We also thank Ms. Eiko Nakajima, Dr. Mayumi Miyamoto, and Ms. Naoko Yasumura for their excellent technical assistance.

Author contributions

K.K., genetic, biochemical, and informatics analysis; T.K., collected the family samples and conducted the histopathological analysis; K.M., iPS biology; H.M., genetic analysis; Y.T., T.M., S.N.A., and S.M., chromosomal analysis of iPS cells; K.M. and M.K., biochemical analysis of cells; M.N., H.M., Y.N., H.I., M.N., A.N., R.I., T.N., M.O., N.E., Y.A., M.A., I.N., Y.I, T.K., M.T., K.S., Y.R., and Y.I., provided samples and clinical information; H.K., K.K., T.K., H.M., and K.M., designed the work and wrote the manuscript with input from all the authors. All the authors read and approved the final manuscript.

Declaration of interests

The authors declare no competing interests.

Received: March 25, 2023
Revised: May 25, 2023
Accepted: May 25, 2023
Published: June 19, 2023

References

1. Love, S., and Greenfield, J.G. (2015). Greenfield's Neuropathology, 9th edition (CRC Press).
2. Goutman, S.A., Hardiman, O., Al-Chalabi, A., Chió, A., Savelieff, M.G., Kiernan, M.C., and Feldman, E.L. (2022). Recent advances in the diagnosis and prognosis of amyotrophic lateral sclerosis. Lancet Neurol. *21*, 480–493.
3. Elden, A.C., Kim, H.J., Hart, M.P., Chen-Plotkin, A.S., Johnson, B.S., Fang, X., Armakola, M., Geser, F., Greene, R., Lu, M.M., et al. (2010). Ataxin-2 intermediate-length polyglutamine expansions are associated with increased risk for ALS. Nature *466*, 1069–1075.
4. DeJesus-Hernandez, M., Mackenzie, I.R., Boeve, B.F., Boxer, A.L., Baker, M., Rutherford, N.J., Nicholson, A.M., Finch, N.A., Flynn, H., Adamson, J., et al. (2011). Expanded GGGGCC hexanucleotide repeat in noncoding region of C9ORF72 causes chromosome 9p-linked FTD and ALS. Neuron *72*, 245–256.
5. Renton, A.E., Majounie, E., Waite, A., Simón-Sánchez, J., Rollinson, S., Gibbs, J.R., Schymick, J.C., Laaksovirta, H., van Swieten, J.C., Myllykangas, L., et al. (2011). A hexanucleotide repeat expansion in C9ORF72 is the cause of chromosome 9p21-linked ALS-FTD. Neuron *72*, 257–268.
6. Hartmann, H., Hornburg, D., Czuppa, M., Bader, J., Michaelsen, M., Farny, D., Arzberger, T., Mann, M., Meissner, F., and Edbauer, D. (2018). Proteomics and C9orf72 neuropathology identify ribosomes as poly-GR/PR interactors driving toxicity. Life Sci. Alliance *1*, e201800070.
7. Mori, K., Weng, S.-M., Arzberger, T., May, S., Rentzsch, K., Kremmer, E., Schmid, B., Kretzschmar, H.A., Cruts, M., Van Broeckhoven, C., et al. (2013). The *C9orf72* GGGGCC repeat is translated into aggregating dipeptide-repeat proteins in FTLD/ALS. Science *339*, 1335–1338.
8. Ishiura, H., Shibata, S., Yoshimura, J., Suzuki, Y., Qu, W., Doi, K., Almansour, M.A., Kikuchi, J.K., Taira, M., Mitsui, J., et al. (2019). Noncoding CGG repeat expansions in neuronal intranuclear inclusion disease, oculopharyngodistal myopathy and an overlapping disease. Nat. Genet. *51*, 1222–1232.

9. Deng, J., Yu, J., Li, P., Luan, X., Cao, L., Zhao, J., Yu, M., Zhang, W., Lv, H., Xie, Z., et al. (2020). Expansion of GGC repeat in GIPC1 is associated with oculopharyngodistal myopathy. Am. J. Hum. Genet. *106*, 793–804.
10. Ogasawara, M., Iida, A., Kumutpongpanich, T., Ozaki, A., Oya, Y., Konishi, H., Nakamura, A., Abe, R., Takai, H., Hanajima, R., et al. (2020). CGG expansion in NOTCH2NLC is associated with oculopharyngodistal myopathy with neurological manifestations. Acta Neuropathol. Commun. *8*, 204.
11. Yu, J., Deng, J., Guo, X., Shan, J., Luan, X., Cao, L., Zhao, J., Yu, M., Zhang, W., Lv, H., et al. (2021). The GGC repeat expansion in NOTCH2NLC is associated with oculopharyngodistal myopathy type 3. Brain *144*, 1819–1832.
12. Yu, J., Shan, J., Yu, M., Di, L., Xie, Z., Zhang, W., Lv, H., Meng, L., Zheng, Y., Zhao, Y., et al. (2022). The CGG repeat expansion in RILPL1 is associated with oculopharyngodistal myopathy type 4. Am. J. Hum. Genet. *109*, 533–541.
13. Zeng, Y.-H., Yang, K., Du, G.-Q., Chen, Y.-K., Cao, C.-Y., Qiu, Y.-S., He, J., Lv, H.-D., Qu, Q.-Q., Chen, J.-N., et al. (2022). GGC repeat expansion of RILPL1 is associated with oculopharyngodistal myopathy. Ann. Neurol. *92*, 512–526.
14. Miyazawa, H., Kato, M., Awata, T., Kohda, M., Iwasa, H., Koyama, N., Tanaka, T., Kyo, S., Okazaki, Y., and Hagiwara, K. (2007). Homozygosity haplotype allows a genomewide search for the autosomal segments shared among patients. Am. J. Hum. Genet. *80*, 1090–1102.
15. Gudbjartsson, D.F., Jonasson, K., Frigge, M.L., and Kong, A. (2000). Allegro, a new computer program for multipoint linkage analysis. Nat. Genet. *25*, 12–13.
16. Matsuda, Y., Morino, H., Miyamoto, R., Kurashige, T., Kume, K., Mizuno, N., Kanaya, Y., Tada, Y., Ohsawa, R., Yokota, K., et al. (2020). Biallelic mutation of HSD17B4 induces middle age-onset spinocerebellar ataxia. Neurol. Genet. *6*, e396.
17. Ng, P.C., and Henikoff, S. (2001). Predicting deleterious amino acid substitutions. Genome Res. *11*, 863–874.
18. Adzhubei, I.A., Schmidt, S., Peshkin, L., Ramensky, V.E., Gerasimova, A., Bork, P., Kondrashov, A.S., and Sunyaev, S.R. (2010). A method and server for predicting damaging missense mutations. Nat. Methods *7*, 248–249.
19. Rentzsch, P., Witten, D., Cooper, G.M., Shendure, J., and Kircher, M. (2019). CADD: predicting the deleteriousness of variants throughout the human genome. Nucleic Acids Res. *47*, D886–D894.
20. Mitsuhashi, S., Frith, M.C., Mizuguchi, T., Miyatake, S., Toyota, T., Adachi, H., Oma, Y., Kino, Y., Mitsuhashi, H., and Matsumoto, N. (2019). Tandem-genotypes: robust detection of tandem repeat expansions from long DNA reads. Genome Biol. *20*, 1–17.
21. De Coster, W., Stovner, E.B., and Strazisar, M. (2020). Methplotlib: analysis of modified nucleotides from nanopore sequencing. Bioinformatics *36*, 3236–3238.
22. Okita, K., Matsumura, Y., Sato, Y., Okada, A., Morizane, A., Okamoto, S., Hong, H., Nakagawa, M., Tanabe, K., Tezuka, K.i., et al. (2011). A more efficient method to generate integration-free human iPS cells. Nat. Methods *8*, 409–412.
23. Okita, K., Yamakawa, T., Matsumura, Y., Sato, Y., Amano, N., Watanabe, A., Goshima, N., and Yamanaka, S. (2013). An efficient nonviral method to generate integration-free human-induced pluripotent stem cells from cord blood and peripheral blood cells. Stem Cell. *31*, 458–466.
24. Ishida, Y., Kawakami, H., Kitajima, H., Nishiyama, A., Sasai, Y., Inoue, H., and Muguruma, K. (2016). Vulnerability of Purkinje cells generated from spinocerebellar ataxia type 6 patient-derived iPSCs. Cell Rep. *17*, 1482–1490.
25. Takahashi, K., Tanabe, K., Ohnuki, M., Narita, M., Ichisaka, T., Tomoda, K., and Yamanaka, S. (2007). Induction of pluripotent stem cells from adult human fibroblasts by defined factors. Cell *131*, 861–872.
26. Lacoste, A., Berenshteyn, F., and Brivanlou, A.H. (2009). An efficient and reversible transposable system for gene delivery and lineage-specific differentiation in human embryonic stem cells. Cell Stem Cell *5*, 332–342.
27. De Santis, R., Garone, M.G., Pagani, F., de Turris, V., Di Angelantonio, S., and Rosa, A. (2018). Direct conversion of human pluripotent stem cells into cranial motor neurons using a piggyBac vector. Stem Cell Res. *29*, 189–196.
28. Garone, M.G., de Turris, V., Soloperto, A., Brighi, C., De Santis, R., Pagani, F., Di Angelantonio, S., and Rosa, A. (2019). Conversion of human induced pluripotent stem cells (iPSCs) into functional spinal and cranial motor neurons using piggyBac vectors. J. Vis. Exp.
29. Rosa, A., Papaioannou, M.D., Krzyspiak, J.E., and Brivanlou, A.H. (2014). miR-373 is regulated by TGFβ signaling and promotes mesendoderm differentiation in human embryonic stem cells. Dev. Biol. *391*, 81–88.
30. Muguruma, K., Nishiyama, A., Kawakami, H., Hashimoto, K., and Sasai, Y. (2015). Self-organization of polarized cerebellar tissue in 3D culture of human pluripotent stem cells. Cell Rep. *10*, 537–550.
31. Muguruma, K., Nishiyama, A., Ono, Y., Miyawaki, H., Mizuhara, E., Hori, S., Kakizuka, A., Obata, K., Yanagawa, Y., Hirano, T., and Sasai, Y. (2010). Ontogeny-recapitulating generation and tissue integration of ES cell-derived Purkinje cells. Nat. Neurosci. *13*, 1171–1180.
32. Kurashige, T., Morino, H., Murao, T., Izumi, Y., Sugiura, T., Kuraoka, K., Kawakami, H., Torii, T., and Maruyama, H. (2022). TDP-43 Accumulation within intramuscular nerve bundles of patients with amyotrophic lateral sclerosis. JAMA Neurol. *79*, 693–701.
33. Brooks, B.R., Miller, R.G., Swash, M., Munsat, T.L.; and World Federation of Neurology Research Group on Motor Neuron Diseases (2000). El Escorial revisited: revised criteria for the diagnosis of amyotrophic lateral sclerosis. Amyotroph. Lateral Scler. Other Motor Neuron Disord. *1*, 293–299.
34. de Carvalho, M., Dengler, R., Eisen, A., England, J.D., Kaji, R., Kimura, J., Mills, K., Mitsumoto, H., Nodera, H., Shefner, J., and Swash, M. (2008). Electrodiagnostic criteria for diagnosis of ALS. Clin. Neurophysiol. *119*, 497–503.
35. Neumann, M., and Mackenzie, I.R.A. (2019). Review: neuropathology of non-tau frontotemporal lobar degeneration. Neuropathol. Appl. Neurobiol. *45*, 19–40.
36. Neumann, M., Sampathu, D.M., Kwong, L.K., Truax, A.C., Micsenyi, M.C., Chou, T.T., Bruce, J., Schuck, T., Grossman, M., Clark, C.M., et al. (2006). Ubiquitinated TDP-43 in frontotemporal lobar degeneration and amyotrophic lateral sclerosis. Science *314*, 130–133.
37. Egawa, N., Kitaoka, S., Tsukita, K., Naitoh, M., Takahashi, K., Yamamoto, T., Adachi, F., Kondo, T., Okita, K., Asaka, I., et al. (2012). Drug screening for ALS using patient-specific induced pluripotent stem cells. Sci. Transl. Med. *4*, 145ra104. https://doi.org/10.1126/scitranslmed.3004052.
38. Sellier, C., Rau, F., Liu, Y., Tassone, F., Hukema, R.K., Gattoni, R., Schneider, A., Richard, S., Willemsen, R., Elliott, D.J., et al. (2010). Sam68 sequestration and partial loss of function

are associated with splicing alterations in FXTAS patients. EMBO J. *29*, 1248–1261.
39. Kumutpongpanich, T., Ogasawara, M., Ozaki, A., Ishiura, H., Tsuji, S., Minami, N., Hayashi, S., Noguchi, S., Iida, A., Nishino, I., et al. (2021). Clinicopathologic features of oculopharyngodistal myopathy with LRP12 CGG repeat expansions compared with other oculopharyngodistal myopathy subtypes. JAMA Neurol. *78*, 853–863.
40. Kremer, E.J., Pritchard, M., Lynch, M., Yu, S., Holman, K., Baker, E., Warren, S.T., Schlessinger, D., Sutherland, G.R., and Richards, R.I. (1991). Mapping of DNA instability at the fragile X to a trinucleotide repeat sequence p(CCG)n. Science (New York, N.Y.) *252*, 1711–1714.
41. Hagerman, R.J., Leehey, M., Heinrichs, W., Tassone, F., Wilson, R., Hills, J., Grigsby, J., Gage, B., and Hagerman, P.J. (2001). Intention tremor, parkinsonism, and generalized brain atrophy in male carriers of fragile X. Neurology *57*, 127–130.
42. Hagerman, R., and Hagerman, P. (2021). Fragile X-associated tremor/ataxia syndrome: pathophysiology and management. Curr. Opin. Neurol. *34*, 541–546.
43. Nobile, V., Pucci, C., Chiurazzi, P., Neri, G., and Tabolacci, E. (2021). DNA methylation, mechanisms of FMR1 inactivation and therapeutic perspectives for fragile X syndrome. Biomolecules *11*, *296*.
44. Rodriguez, C.M., Wright, S.E., Kearse, M.G., Haenfler, J.M., Flores, B.N., Liu, Y., Ifrim, M.F., Glineburg, M.R., Krans, A., Jafar-Nejad, P., et al. (2020). A native function for RAN translation and CGG repeats in regulating fragile X protein synthesis. Nat. Neurosci. *23*, 386–397.
45. Beckers, J., Tharkeshwar, A.K., and Van Damme, P. (2021). C9orf72 ALS-FTD: recent evidence for dysregulation of the autophagy-lysosome pathway at multiple levels. Autophagy *17*, 3306–3322.
46. Saito, R., Shimizu, H., Miura, T., Hara, N., Mezaki, N., Higuchi, Y., Miyashita, A., Kawachi, I., Sanpei, K., Honma, Y., et al. (2020). Oculopharyngodistal myopathy with coexisting histology of systemic neuronal intranuclear inclusion disease: Clinicopathologic features of an autopsied patient harboring CGG repeat expansions in LRP12. Acta Neuropathol. Commun. *8*, 75.